# A First-Principles Modeling of Ni Interactions on CeO$_2$–ZrO$_2$ Mixed Oxide Solid Solutions

Federico Cova,[†] Delfina García Pintos,[†] Alfredo Juan,[‡] and Beatriz Irigoyen[*,†]

[†]Departamento de Ingeniería Química, Facultad de Ingeniería, Universidad de Buenos Aires, Pabellón de Industrias, Ciudad Universitaria, (1428) Capital Federal, Argentina

[‡]Departamento de Física, Universidad Nacional del Sur, Avda. Alem 1253, (8000) Bahía Blanca, Argentina

ABSTRACT: We performed DFT+U quantum period calculations to study the characteristics of Ni interactions on/in CeO$_2$–ZrO$_2$ mixed oxide solid solutions. We analyzed the energetics of Ni adsorption and insertion on/in different surface and subsurface sites of the Ce$_{0.25}$Zr$_{0.75}$O$_2$(111) slab, and also the changes in its atomic and electronic structures. The most stable interaction corresponds to a single Ni atom adsorbed on the O–O bridge site, where the nearest-neighbor metal atom is the Zr. Our calculations also show that Ni can form small clusters on the Ce$_{0.75}$Zr$_{0.25}$O$_2$(111) surface; which also locate around the Zr dopant. Due to Ni interactions, surface and inner layers oxygen anions experience important modifications in their geometric positions and the Ni atom deposition results in the partial occupation of 7-coordinated Ce(4f) states.
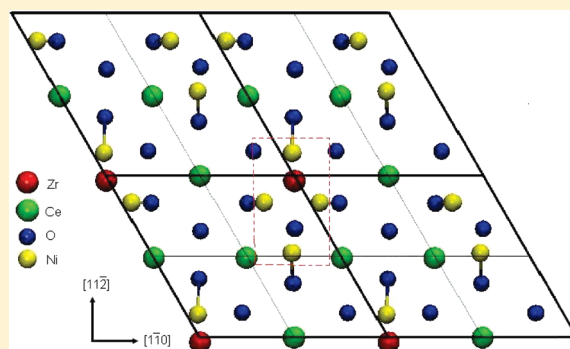
1. INTRODUCTION

Cerium oxide-based materials are extensively used as catalysts for purification of exhaust gases in the three-way automotive converts, combustion of organics, production and purification of hydrogen, water gas shift reaction, selective oxidation of CO, production of synthesis gas (syngas), or gas sensors.[1–3]

Syngas, a mixture of carbon monoxide and hydrogen, is not only easily converted to hydrogen through the water gas shift reaction, but also is a fundamental feedstock for the production of methanol, dimethyl ether, and Fischer–Tropsch liquid fuels.[4,5] The predominant processes involved in the production of synthesis gas are catalytic partial oxidation and steam and dry reforming of methane, and also steam reforming of other hydrocarbons and alcohols. Industrially, the catalysts commonly employed in these processes are based on massive or supported Ni, Pd, Pt, and Rh. The noble metals Pd, Pt, and Rh are more stable and active than Ni. However, Ni is the cheapest and therefore the most abundant element in the composition of commercial catalysts.

The catalytic performance of Ni can be improved by the addition of another metal or by the use of reducible supports. Ni supported on pure CeO$_2$ catalysts has shown good activity for methane partial oxidation reactions, but it rapidly deactivated due to severe surface carbon deposition.[6] Besides, pure CeO$_2$ supports presented poor thermal resistance and stability at high-temperature operation conditions. The performance of cerium oxide, mainly related to Ce^{4+}/Ce^{3+} couples, reduction facility and oxygen mobility properties, has been improved by the addition of transition, alkaline-earth, or rare-earth metals.[1,7] The incorporation of those metals into the CeO$_2$ lattice enhanced

its redox properties, oxygen mobility, and thermal stability. Particularly, the doping of CeO$_2$ with Zr promoted its Ce^{4+}/Ce^{3+} couples, oxygen storage capacity, thermal resistance, and catalytic activity.[8–12] CeO$_2$–ZrO$_2$ solid solutions showed better thermodynamic properties than pure CeO$_2$, because of their improved redox couples formation and reversible oxygen storage properties.[13–15] Consequently, Ni/CeO$_2$–ZrO$_2$ solid solutions have exhibited excellent catalytic behavior during methane reforming reactions.[16–28]

The performance of Ni/CeO$_2$–ZrO$_2$ catalysts with different contents of Zr has been compared to that of Ni supported on pure CeO$_2$ or ZrO$_2$ oxides, for partial oxidation of methane.[19] Ni/CeO$_2$–ZrO$_2$ samples presented higher activity, lower reaction temperature, and excellent coking resistance, and these remarkable catalytic characteristics were related to their physics construction and also to strong Ni interactions with the CeO$_2$–ZrO$_2$ supports. Ni/CeO$_2$, Ni/ZrO$_2$, and Ni/Ce$_{0.8}$Zr$_{0.2}$O$_2$ catalysts have been evaluated for combined reforming of methane to produce synthesis gas for gas to liquid (GTL) process.[22] The authors related the enhanced catalytic activity and stability of Ni/Ce$_{0.8}$Zr$_{0.2}$O$_2$ catalyst to the combination of cubic Ce$_{0.8}$Zr$_{0.2}$O$_2$ mixed oxide and finely dispersed nanosized NiO crystallites, which resulted in intimate contact between Ni and the support, better Ni dispersion, and improved oxygen transference during the reactions. Ni/CeO$_2$–ZrO$_2$ catalyst, compared to the ZrO$_2$-free sample, exhibited much higher activity for dry reforming of

methane reactions.[23] This was attributed to the presence of Zr in the support, which considerably altered the electronic environment of the Ce ions, increasing the concentration of the active sites of the surface. Besides, $Ni/Ce_{0.9}Zr_{0.1}O_2$ solid solution has been reported as very promising anode material for hydrogen production from methane partial oxidation, for power generation in solid oxide fuel cells operating at intermediate temperatures.[24,25] On the other hand, the relationship between activity and coke formation in Ni/CeO_2-based catalysts has been also investigated.[26] The authors reported, from samples characterization and methane dry reforming tests, an active role of CeO_2-ZrO_2 mixed oxides in the gasification of surface coke. The strong interactions between Ni and Ce—Zr supports have been identified as responsible for coke deposition prevention.[27,28] Besides, $Ni/Ce_{1-x}Zr_xO_2$ ($x = 0$, 0.25, 0.5, 0.75, 1) catalysts, with finely dispersed Ni particles on their surfaces, exhibited high activity and resistance to carbon deposits formation.[19,20] The coking resistance of $Ni/Ce_{0.75}Zr_{0.25}O_2$ catalyst has been compared with that of Ni/CeO_2 and Ni/ZrO_2 catalysts for methane partial oxidation to synthesis gas reactions.[20] $Ni/Ce_{0.75}Zr_{0.25}O_2$ mixed oxide resisted coke formation more than the other catalysts, mainly because of the high degree of Ni dispersion and surface oxygen mobility.

The difference between Ni interactions with CeO_2-ZrO_2 mixed oxides and that with undoped CeO_2 supports are highly relevant to catalysis, as previously discussed. In spite of that, the catalytic behavior of Ni/CeO_2-ZrO_2 solid solutions is still not fully understood and more research is needed to improve their comprehension. Computational chemistry calculations on such materials can provide information at atomic level about the metal—support interactions, and the changes introduced in the geometric and electronic structures of the support by the presence of the promoter. These insights would be also very useful for the design of new Ni/CeO_2-based oxides catalysts, which need to fulfill two main requirements: resistance to carbon deposition and stability against metal particles sintering.

Theoretically, many works have reported electronic and geometric studies on bare CeO_2 and ZrO_2 solids, and also on noble metals supported on those oxides.[29−33] Besides, the interfacial properties of Pd and Pt supported on $Ce_{0.25}Zr_{0.75}O_2$ systems were evaluated by first-principles electronic structure calculations.[34] The density functional theory has been applied to study the defect chemistry and electronic structure of Ni/CeO_2 materials.[35] Recently, the effects of Ni substitutional and interstitial point defects in CeO_2 structure were investigated by performing ab initio calculations.[36] However, as far as we know, there are no publications that provide first-principles insights about Ni/CeO_2-ZrO_2 systems, which can help to explain Ni particles dispersion and oxygen mobility characteristics of these materials. Therefore, in this work we performed density functional calculations to investigate the energetics of Ni adsorption/insertion on/in different $Ce_{0.75}Zr_{0.25}O_2(111)$ sites, and the changes in the geometric and electronic structure of the Ce—Zr mixed oxide support.

2. COMPUTATIONAL METHOD

We performed plane-wave periodic density functional (DFT) calculations implemented with the Vienna Ab-initio Simulation Package (VASP).[37,38] The Kohn—Sham equations were solved with the generalized gradient approximation (GGA) using the exchange-correlation functional of Perdew—Burke—Ernzerhof (PBE).[39]

The core electrons were represented with the projector augmented wave (PAW) method.[40] The valence electron wave functions were expanded using a truncation energy value of 400 eV, and the tolerance for the total free energy change set in 10^{-4} eV. We have used the valence configurations 5s, 5p, 5d, 4f, 6s for cerium; 2s, 2p for oxygen; 5s, 4d, 5p for zirconium; and 4s, 3d for nickel. The Brillouin zone was sampled with a $4 \times 4 \times 1$ k-points grid according to the Monkhorst—Pack scheme,[41] and a Gaussian smearing of 0.2 eV. For the energy calculations, we considered spin polarization effects and the final results were extrapolated to those of SIGMA = 0 eV.

The standard DFT formulation usually fails to describe strongly correlated electrons due to a deficient treatment of electron correlation. This limitation has been corrected by using the DFT+U method, where the introduction of a Hubbard parameter U modified the self-interaction error and enhanced the description of the correlation effects.[42,43] In this work, we used a Hubbard parameter $U = 5$ eV to describe the on-site Coulomb interaction of the Ce(4f) electrons. This value is consistent with the recommendations of Nolan et al., who have reported that CeO_2 structure essentially converges with respect to localization for a value of the U parameter greater or equal to 5.0 eV.[44,45]

Cerium oxide has a fluorite structure (CaF_2), consisting of a cubic close-packed array of Ce cations with all tetrahedral holes filled by O anions. In the fluorite-type structure, each Ce^{4+} cation is surrounded by eight O^{2-} anions, which form the corners of a cube. Also, each O^{2-} anion is surrounded by four metal cations in a tetrahedron-like structure.

The reported experimental value of the CeO_2 lattice parameter is 5.41 Å.[46] Besides, experimental studies have indicated that cubic lattice parameter of CeO_2 decreased due to Zr mixing into the cerium oxide.[3,47]

In this work, we simulated the $Ce_{0.75}Zr_{0.25}O_2$ solid solution by introducing a Zr-dopant atom into the bulk cubic cell of CeO_2, as reported in ref 7. The doped system contains 25% of Zr ions in each of the cation layers, and our calculated DFT value of the lattice constant is 5.41 Å (5.42 Å, in ref 7).

For cerium oxide, it has been reported that $CeO_2(111)$ face is the most stable.[3,48] This surface corresponds to the minimal Ce—O bond's cleavage. Thus, we performed Ni adsorption calculations on the (111) face of the Ce—Zr solid solution doped with 25% Zr.

The $Ce_{0.75}Zr_{0.25}O_2$ (111) surface was modeled as a supercell (see Figure 1). This system, obtained by cleaving the optimized bulk cell, was simulated with a 12-atomic-layer slab. The dimensions of the supercell, $7.65 \times 7.65 \times 22.80$ Å^3, avoided periodic interactions of adsorbed molecules with the atoms of the upper layers. Also, we allowed the layers to relax from top to sixth, and fixed the next six layers to the bulk value. After that, we optimized the geometry for the Ce, Zr, and O ions in the relaxed layers until the forces on atoms were less than 0.02 eV/Å.

The Ni atom adsorption energy was calculated as the difference between the total free energy of the $Ni/Ce_{0.75}Zr_{0.25}O_2(111)$ system and that of the bare $Ce_{0.75}Zr_{0.25}O_2(111)$ surface terminated by oxygen atoms and the atomic nickel:
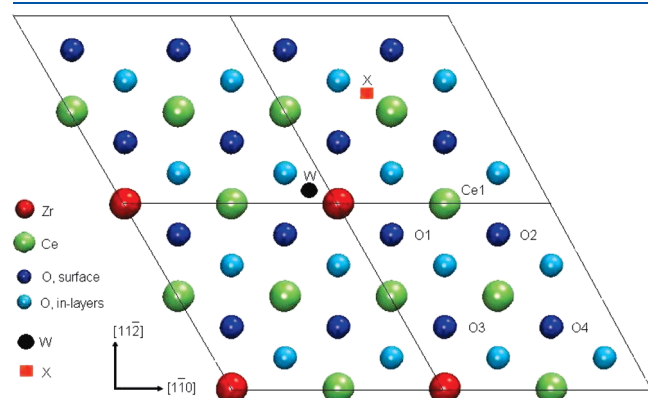
$$\Delta E_{ads,Ni} = E[Ni/Ce_{0.75}Zr_{0.25}O_2(111)$$

$$- E[Ce_{0.75}Zr_{0.25}O_2(111)] - E[Ni]$$

A negative value of $\Delta E_{ads,Ni}$ means that Ni interaction on the surface sites is stable. The value of the atomic nickel energy was taken as the lowest triplet state Ni d^9, s^1: $E[Ni] = -0.52$ eV.[36,49]

7457

dx.doi.org/10.1021/jp1108703 |J. Phys. Chem. C 2011, 115, 7456–7465

We studied Ni atom interactions on different sites of the $Ce_{0.75}Zr_{0.25}O_2(111)$ surface. Four of these sites are positions on top of Ce, Zr, O1, and O4 ions (see Figure 1), and the other two are bridge positions above two surface oxygen anions (the O−OP bridge sites W and X).

The oxygen anions O1, O2, and O3 are located over the center of a triangle which corners are occupied by Ce and Zr cations. However, the O4 anion is located over the center of a triangle which corners are only occupied by Ce cations. Thus, we studied Ni adsorption on top of the O1-type and O4 oxygen atoms.

The sites W and X are bridge positions above two oxygen anions O2 and O3. As we can see in Figure 1, the environments of these sites are different. On the site W, the nearest-neighbor metal atom is a Zr cation; while on the site X, it is a Ce cation.

Figure 1. Top view of the bare $Ce_{0.75}Zr_{0.25}O_2(111)$ face, with indication of the studied Ni surface adsorption sites: Ce, Zr, O1, O4, and O−O positions W and X.

Table 1. Adsorption Energy Value for a Single Ni Atom Interacting on the $Ce_{0.75}Zr_{0.25}O_2(111)$ Surface

Ni positions	$\Delta E_{ads,Ni}$ (eV)
on top of Ce	−0.47
on top of oxygen O4	−2.48
on top of oxygen O1	−2.77
on top of Zr	−3.21
on the O−O bridge X	−3.88
on the O−O bridge W	−4.21

Thus, we calculated Ni interactions on the O−O bridge sites W and X.

We also evaluated other possible locations of Ni on the $Ce_{0.75}Zr_{0.25}O_2(111)$ surface such as Ce−O bridge, Zr−O bridge, Ce−Ce bridge, Ce−Zr bridge, and hollow sites. Our results indicated that these optimized systems would relax into one of the aforementioned structures.

3. RESULTS AND DISCUSSION

In the following, we discuss the mechanistic details of Ni interactions on/in different $Ce_{0.75}Zr_{0.25}O_2(111)$ surface and subsurface sites.

3.1. Interactions of a Single Ni Atom on the $Ce_{0.75}Zr_{0.25}O_2$-(111) Surface. The calculated energy values for the adsorption of Ni on different $Ce_{0.75}Zr_{0.25}O_2(111)$ surface sites were reported in Table 1. The less favorable energy value for the Ni adsorption corresponds to a single Ni atom located on top of surface cerium cations, where the Ni−Ce repulsion is maximized.[35] Nickel interactions on Zr and O ions are stable, and the order of preference for Ni adsorption on the different surface sites is: O top < Zr top < O−O bridge.

When Ni was placed on top of oxygen O1, which coordinates with a Zr cation, a Ni−O bond of 1.78 Å was formed after the relaxation (see Table 2). As a result, the oxygen O1 was moved outward the surface about 0.3 Å (see Figure 2). The rise of the other surface oxygen ions was lower than that of O1; oxygens O2 and O3 were moved up 0.07 and 0.13 Å, respectively. The oxygen O4 relaxed only on the (111) plane; it was moved 0.12 Å toward the oxygen O1. Those surface oxygen movements also affected the O anions located on the third layer, which were displaced 0.1 Å on its plane. The nearest-neighbor cations of oxygen O1 showed lower displacements: Zr was moved down 0.04 Å, while Ce was raised 0.07 Å (see Figure 2). The movement of oxygen

Table 2. Ni−O Bond Lengths for a Single Ni Atom Adsorbed on the $Ce_{0.75}Zr_{0.25}O_2(111)$ Surface

Ni positions	d(Ni−O) (Å)
on top of oxygen O1	1.78
on top of oxygen O4	1.78
on the O−O bridge site X	1.87, 1.94
on the O−O bridge site W	1.86, 1.92
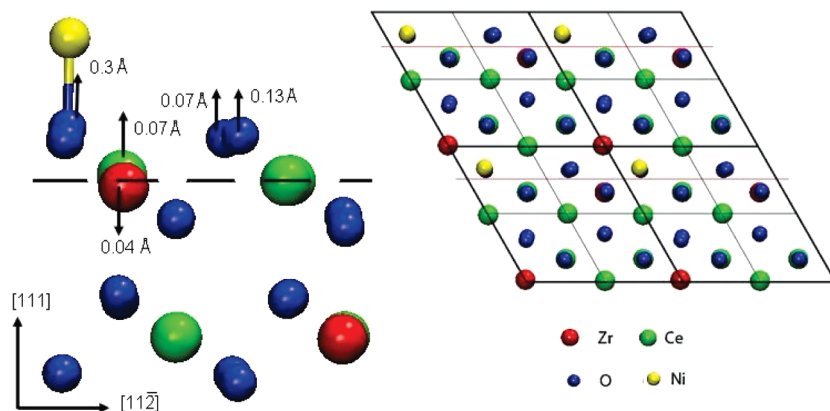
Figure 2. Side view of the relaxation caused by Ni adsorption on top of the oxygen O1 on the $Ce_{0.75}Zr_{0.25}O_2(111)$ surface. The dotted line indicates the position of the top metal cations. The region shown in the side view is also indicated between red lines in the front view on the right.

O1, away from the surface, also influenced the Zr−O1 bond stability; the O1−Zr distance elongated 0.14 Å (see Table 3).

Ni interaction on top of oxygen O4 led to a Ni−O4 bond length similar to that of Ni−O1 (see Table 2: d(Ni−O4) = d(Ni−O1) = 1.78 Å). Also, the movements of the surface and third layer oxygen ions were similar to those observed for Ni adsorption on top of oxygen O1. On the other hand, no displacement of the two Ce cations nearest neighbors of oxygen O4 was observed.

We report in Tables 3 and 4 Zr−O and Ce1−O bonds length for the bare $Ce_{0.75}Zr_{0.25}O_2(111)$ surface and after Ni adsorption on top of oxygens O1 and O4. We can see that the most significant change is that of Ce1−O1 bond, which was elongated 21% after Ni−O1 bond formation. The nearest-neighbor metal cations of oxygen O1 are one Zr and two Ce, while oxygen O4 is surrounded by three Ce cations.

Table 3. Zr−O Distances on $Ce_{0.75}Zr_{0.25}O_2(111)$ and Ni−$Ce_{0.75}Zr_{0.25}O_2(111)$ Surfaces

	d(Zr−O1) (Å)	d(Zr−O2) (Å)	d(Zr−O3) (Å)
bare surface	2.48	2.48	2.16
Ni on top of oxygen O1	2.62	2.72	2.17
Ni on top of oxygen O4	2.60	2.60	2.12
Ni on top of Ce	2.52	2.52	2.16
Ni on top of Zr	2.24	2.29	2.31
Ni on the O−O bridge site X	2.13	2.27	3.73
Ni on the O−O bridge site W	2.14	2.17	3.19

Table 4. Ce1−O Distances on $Ce_{0.75}Zr_{0.25}O_2(111)$ and Ni/$Ce_{0.75}Zr_{0.25}O_2(111)$ Surfaces

	d(Ce1−O1) (Å)	d(Ce1−O2) (Å)	d(Ce1−O4) (Å)
bare surface	2.14	2.14	2.36
Ni on top of oxygen O1	2.59	2.12	2.46
Ni on top of oxygen O4	2.53	2.05	2.57
Ni on top of Ce	2.51	2.18	2.46
Ni on top of Zr	2.62	2.11	2.44
Ni on the O−O bridge site X	2.50	2.25	2.38
Ni on the O−O bridge site W	2.47	2.00	2.39

Theoretical DFT+U calculations have shown that oxygen vacancy is more easily created on those $CeO_2(111)$ surface sites located near Zr centers.[7,50] Thus, the localization of the Zr dopant near oxygen O1 could explain that Ni interaction on top of oxygen O1 was about 0.3 eV stronger than that on top of oxygen O4.

We also studied the Ni interaction on top of Zr cation, which was 0.44 eV more stable than that on top of oxygen O1 (see Table 1). The Zr was moved inward the bulk by 0.19 Å and the three oxygens located near the Zr cation were moved 0.25−0.37 Å out of the surface (see Figure 3). These oxygens were also displaced on the (111) plane by 0.11−0.18 Å (see Figure 4) and became located near the Ni atom at distances of 2.09−2.23 Å. Also, the Zr−O1 and Zr−O2 distances were shortened due to Ni interaction over Zr (see Table 3).

We also studied Ni interactions on the bridge position above the two oxygen atoms of the $Ce_{0.75}Zr_{0.25}O_2(111)$ surface. When the Ni atom was adsorbed on the O−O bridge site W, the Zr was moved down 0.18 Å toward an oxygen anion of the third layer (see Figure 5). The two surface oxygens O2 and O3 were moved out of the surface and bonded to the Ni atom. These oxygen anions and the nearest Zr cation were also relaxed on the (111) plane, as shown in Figure 6. The Ni−O distances, 1.86 and 1.92 Å, respectively (see Table 2), are larger than that found after Ni adsorption on top of oxygen O1 (1.78 Å). On the other hand, the relaxation of the $Ce_{0.75}Zr_{0.25}O_2(111)$ structure due to the adsorption of Ni atom on the O−O bridge site X, which nearest-neighbor metal cation is a Ce, was similar to that resulting from Ni adsorption on the site W. The comparison of the calculated adsorption energy values for these two interactions (see Table 1) showed that Ni adsorption on the O−O bridge site W is 0.33 eV more stable than that on the site X. The energetic of the most favorable of these interactions, Ni adsorption on the O−O bridge site W, was driven by the location of the Ni atom: close to a Zr and far away from Ce ions, thus minimizing Ni−Ce repulsive interactions.[35]

3.2. Interactions of Two Ni Atoms on the $Ce_{0.75}Zr_{0.25}O_2$-(111) Surface. The adsorption of two Ni atoms (Ni_2) on the $Ce_{0.75}Zr_{0.25}O_2(111)$ surface was also considered, in order to compare their relative stabilities. For that purpose, we placed a second Ni atom on the $Ce_{0.75}Zr_{0.25}O_2(111)$ surface with a Ni adsorbed on the most favorable O−O bridge site W position previously found ($Ni_W/Ce_{0.75}Zr_{0.25}O_2$). The value of Ni adsorption
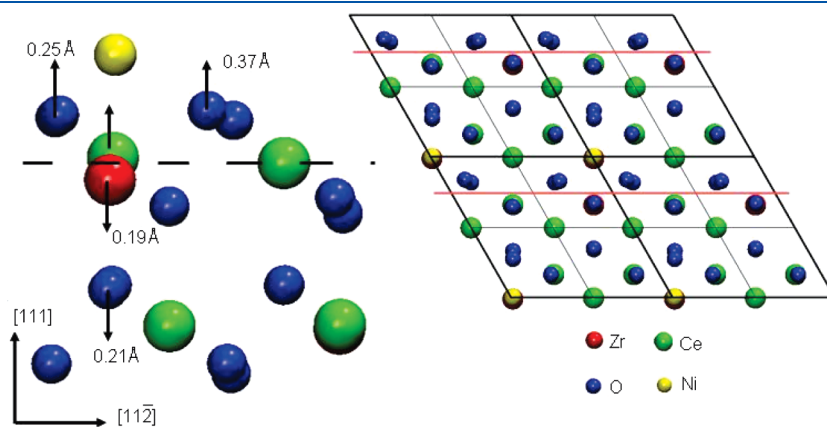
Figure 3. Side view of the relaxation caused by Ni adsorption on top of a Zr cation on the $Ce_{0.75}Zr_{0.25}O_2(111)$ surface. The dotted line indicates the position of the top metal cations. The region shown in the side view is also indicated between red lines in the front view on the right.
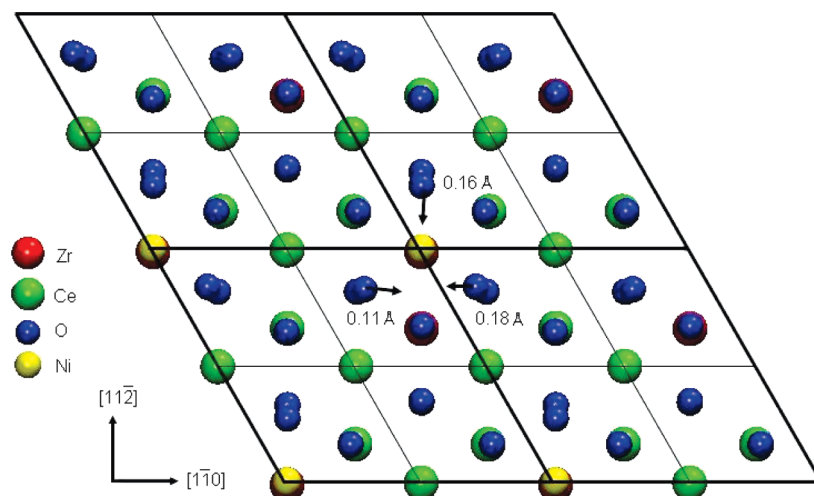
Figure 4. Front view of the relaxation caused by Ni adsorption on top of a Zr cation on the $Ce_{0.75}Zr_{0.25}O_2(111)$ surface.
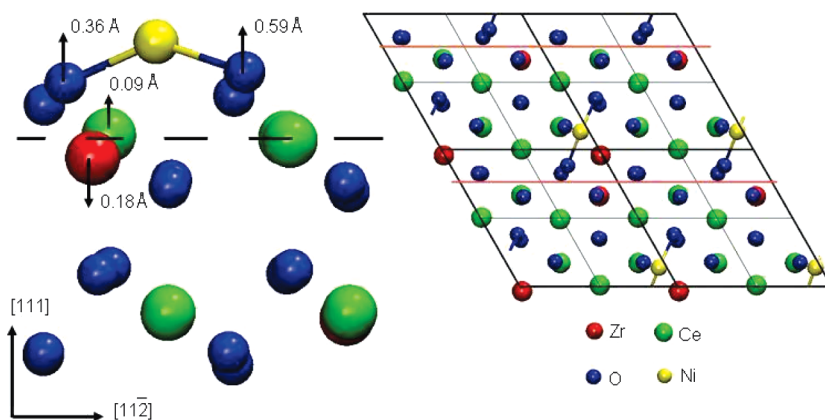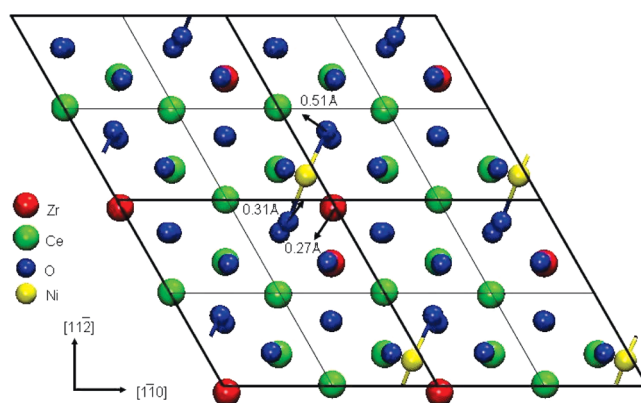

Figure 5. Side view of the relaxation caused by Ni adsorption on the O−O bridge site W on the $Ce_{0.75}Zr_{0.25}O_2(111)$ surface. The dotted line indicates the position of the top metal cations. The region shown in the side view is also indicated between red lines in the front view on the right.

energy (eV/Ni atom) was calculated as

$$\Delta E_{ads, Ni} = \{E[Ni_2/Ce_{0.75}Zr_{0.25}O_2(111)] \\ - E[Ce_{0.75}Zr_{0.25}O_2(111)] - 2E[Ni]\}/2$$

Due to the interaction of the second Ni atom on the O−O bridge site X, the surface oxygens O2 and O3 were moved 1.35 Å out of the surface. As a result, four Ni−O bonds of similar length were formed (see Table 5). We also observed the relaxation of the geometric positions of oxygen atoms located on the third layer. The calculated adsorption energy value for this interaction was $\Delta E_{ads,Ni} = -2.35$ eV/Ni atom (see Table 6).

In the case of the deposition of a second Ni atom on the site W, the interaction was more favorable with an adsorption energy value $\Delta E_{ads,Ni} = -2.83$ eV/Ni atom (see Table 6). The lengths of the formed Ni−O bonds, in the range of 1.83−1.93 Å, are reported in Table 5. The optimization of this structure involved surface relaxation of the geometric positions of surface O, Ce, and Zr ions and also subsurface inner layers oxygens. The surface oxygens O2 and O3 were raised 0.6 Å (see Figure 7). In addition, the movements of the oxygen anions were extended to those in the third and four layers of the slab. In spite of that extended relaxation of O, Ce, and Zr atomic positions, no reconstruction of the CeO_2−ZrO_2 support crystal structure was observed.

Figure 6. Front view of the relaxation caused by Ni adsorption on the O−O bridge site W on the $Ce_{0.75}Zr_{0.25}O_2(111)$ surface.

The calculated adsorption energy value for the second Ni on the O−O bridge site W was about 67% of that found for a single Ni atom on the same site on the bare surface.

3.3. Interactions of a Ni Atom into the $Ce_{0.75}Zr_{0.25}O_2(111)$ Slab. We also compared Ni interactions in the Ce−Zr(111) subsurface layers with those on the surface. We calculated the

nickel absorption energy by placing a Ni atom in different positions into the $Ce_{0.75}Zr_{0.25}O_2(111)$ slab: (i) in the subsurface layer, (ii) between the first metal cations (Ce and Zr) layer and the second oxygen layer, and (iii) between the second and third oxygen layers. Similarly to the previous DFT calculations, we performed structure relaxations by keeping fixed the in-plane lattice vectors. The most favorable interaction corresponded to the insertion of the Ni atom in the plane between the second and third oxygen layers. The calculated energy value for this Ni interaction was $\Delta E_{abs,Ni} = -3.88$ eV, only 0.33 eV higher than that for a Ni atom deposition on the surface O—O bridge site W. Thus, a single Ni atom insertion and adsorption interactions were almost comparable for the Zr-doped CeO_2 system.

After Ni insertion in the plane between the second and third oxygen layers, the spacing between these layers (1.5 Å in the Ce—Zr bare slab) increased to 2.18 Å. The Ni atom, inserted about 2.4 Å below the surface, coordinated with two oxygen anions of the second O-layer and with one oxygen of the third O-layer: $d(Ni-O_{second\ layer}) = 1.96$ and 2.07 Å, and $d(Ni-O_{third\ layer}) = 2.03$ Å. These Ni—O distances are similar to the Ni—O bond lengths in the nickel oxide (2.08 Å). The nearest-neighbor metal cations of Ni atom were located on the fifth layer of the slab. The Ni—Ce distance was 3.95 Å, larger than that for the Ni_2Ce alloy (about 3 Å, see ref 51); while the Ni—Zr distance was 2.8 Å.
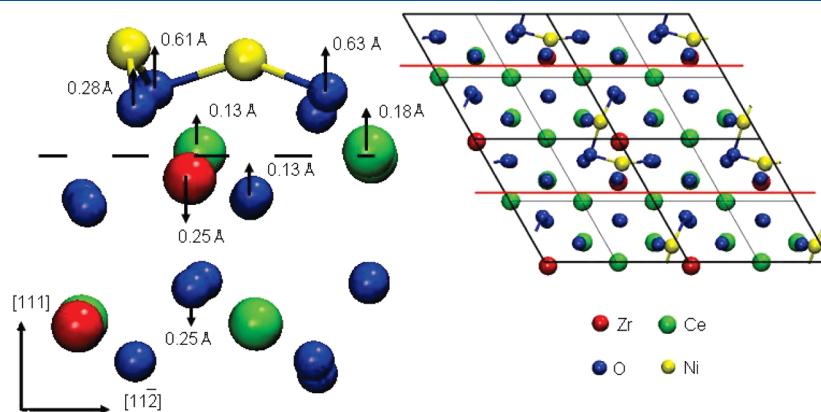
Next, we evaluated the possibility of a Ni insertion into the Ce—Zr slab after Ni atoms deposition on its surface. The most favorable absorption/adsorption sites previously found were only considered. Thus, we placed a Ni atom into the second and third oxygen layers of the $Ce_{0.75}Zr_{0.25}O_2(111)$ support with two Ni atoms adsorbed on the O—O bridge sites W and

W. Then we relaxed the positions of the Ni atoms together with that of the Ce, Zr, and O ions located on the six top atomic layers of the Ce—Zr slab model. The energy value for this Ni interaction was calculated as the difference between the total free energy of the $Ni^*/Ce_{0.75}Zr_{0.25}O_2(111)^{**}$ system and that of the $Ce_{0.75}Zr_{0.25}O_2(111)^{**}$ slab and the atomic Ni energy. Ni^* represents a Ni atom inserted into the $Ce_{0.75}Zr_{0.25}O_2(111)^{**}$ slab subsurface layers, while $Ce_{0.75}Zr_{0.25}O_2(111)^{**}$ represents the $Ce_{0.75}Zr_{0.25}O_2(111)$ slab with two Ni atoms adsorbed on its surface (each one over an O—O bridge site W). The calculated Ni absorption energy value after structure relaxation was $\Delta E_{abs,Ni} = -0.92$ eV. The insertion of a Ni atom into the Ce—Zr slab with Ni deposited on its surface was 2.97 eV less favorable than that into the bare Ce—Zr slab.

3.4. Interactions of Ni Clusters on the $Ce_{0.75}Zr_{0.25}O_2(111)$ Surface. Finally, we compared the relative stability of nickel clusters versus a single Ni atom deposition on the CeO_2-ZrO_2 surface. We calculated the adsorption energy for the adsorption of four Ni atoms (Ni_4) on the $Ce_{0.75}Zr_{0.25}O_2(111)$ supercell. The Ni atoms were placed atop the surface oxygens on the CeO_2-ZrO_2 support, and then optimized their positions together with those of the Ce, Zr, and O ions located on the top six atomic layers of the slab.

The Ni adsorption energy (eV/Ni atom) was evaluated as

$$\Delta E_{ads,Ni} = \{E[Ni_4/Ce_{0.75}Zr_{0.25}O_2(111)]$$
$$- E[Ce_{0.75}Zr_{0.25}O_2(111)] - 4E[Ni]\}/4$$

The interaction of four Ni atoms on the $Ce_{0.75}Zr_{0.25}O_2(111)$ surface was favorable, with an energy value of $\Delta E_{ads,Ni4} = -3.89$ eV/Ni atom. In Figure 8 we can see that the optimization of this geometry ended with the four Ni atoms located around the Zr dopant. Moreover, the oxygens O1, O2, and O3 were relaxed to positions at the hole above a subsurface oxygen atom. These oxygen atoms were moved to that hole by 0.14, 0.15, and 0.45 Å, respectively; while the Zr cation was displaced 0.16 Å to the center of the Ni cluster.

The Ni atoms chemisorbed to the surface oxygens by forming four Ni—O bonds of 1.78, 1.81(2), and 1.83 Å, respectively. As a result, the oxygens O1, O2, and O4 were moved out of the surface by 0.27, 0.28, and 0.40 Å, respectively (see Figure 9). The oxygen O3 was the most relaxed surface anion; it was raised by 0.7 Å, and also moved 0.45 Å away from the Zr cation. The movements of the surface oxygens also modified the atomic

Table 5. Ni—O Bond Lengths for Two Ni Atoms Adsorbed on the $Ce_{0.75}Zr_{0.25}O_2(111)$

Ni positions	$d(Ni-O)$ (Å)
Ni on the O—O bridge sites X and W	1.73 (2), 1.74 (2)
Ni on the O—O bridge sites W and W	1.83, 1.89, 1.92, 1.93

Table 6. Adsorption Energy Values for Two Ni Atoms Interacting on the $Ce_{0.75}Zr_{0.25}O_2(111)$ Surface

Ni positions	$\Delta E_{ads,Ni}$ (eV/Ni atom)
Ni on the O—O bridge sites X and W	−2.35
Ni on the O—O bridge sites W and W	−2.83

Figure 7. Side view of the relaxation caused by Ni adsorption on O—O bridge sites W and W on the $Ce_{0.75}Zr_{0.25}O_2(111)$ surface. The dotted line indicates the position of the top metal cations. The region shown in the side view is also indicated between red lines in the front view on the right.

7461

dx.doi.org/10.1021/jp1108703 |*J. Phys. Chem. C* 2011, 115, 7456–7465

positions of the oxygens located on the third and fourth O-layers. These oxygens were displaced on its plane about 0.3 Å, and also moved 0.14 Å up to the surface, or 0.18 Å toward the bulk (see Figure 9). In addition, the Zr cation was moved 0.17 Å down to the subsurface. On the other hand, the atomic positions of Ce cations remained almost unchanged.

The significant exothermic interaction of Ni_4 species and the meaningful relaxation of the structure of the CeO_2-ZrO_2 support indicated that Ni could stabilize on the $Ce_{0.75}Zr_{0.25}O_2(111)$ surface in the form of small supported Ni clusters located around the Zr dopant. This idea was also supported by the calculated Ni_4 tetrahedron cohesive energy value of -2.43 eV/Ni atom, and the Ni−Ni bond distances which lay in a range of $2.25-2.36$ Å in the optimized Ni_4 cluster. Thus, the Zr dopant could act as nucleation centers for Ni clustering.

3.5. Effect of Ni Deposition on the Electronic Structure of the $Ce_{0.75}Zr_{0.25}O_2(111)$ Surface. Our theoretical study of Ni interactions on the $Ce_{0.75}Zr_{0.25}O_2(111)$ slab showed that Ni bonded preferentially to the oxygens located near a Zr dopant. The calculations also showed that these oxygens were partially moved away from the surface. Thus, we analyzed the density of states (DOS) of this system in order to understand the electronic effect of Ni adsorption on the $Ce_{0.75}Zr_{0.25}O_2(111)$. The DOS curve (see Figure 10) showed the typical highest occupied valence band made mainly of O(2p) orbitals, and the narrow Ce(4f) empty conduction band. The Ce(5d) and Ce(6s) states were located higher in energy than the Ce(4f) states. This
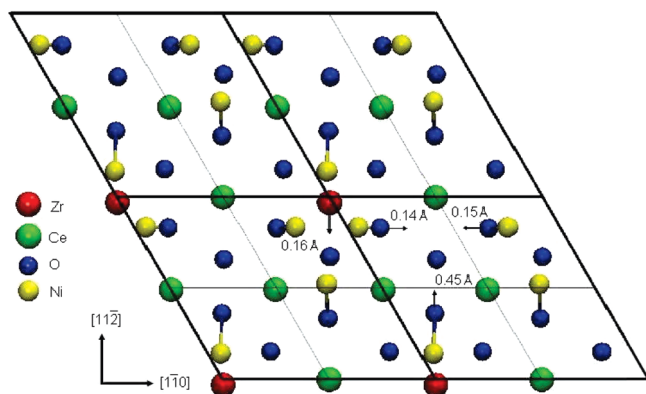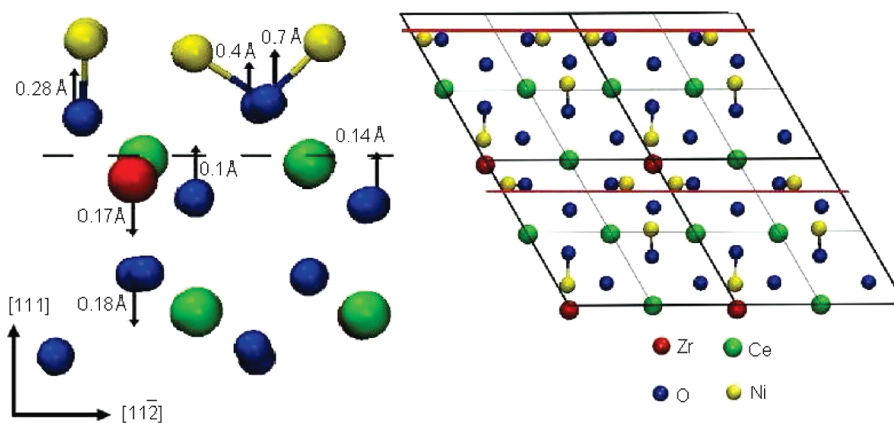
manifold is consistent with the reported electronic structure of the $Ce_{0.75}Zr_{0.25}O_2(111)$ bare surface (see ref 31). The computed energy value of the gap between the top of the valence band and the bottom of conduction band was 2.1 eV, while the reported experimental value for the bare mixed oxide gap is 3.0 eV.[52]

The DOS plot of the $Ni_W/Ce_{0.75}Zr_{0.25}O_2(111)$ system also showed new peaks located between the top of the valence band and the bottom of the conduction band. The wide peak at lower energy was made mainly from Ni(3d) and O(2p) contributions. This peak corresponded to the Ni(3d)−O(2p) overlapping and reflects the Ni-bonding interactions with surface oxygens. The sharp peak at higher energy was located 0.83 eV below the main 4f manifold. Our calculations showed that this peak was made of Ce(4f) orbitals and originated by the metal−support interaction, with the Ni atom pulling of surface oxygens. The electron transference to the hepta-coordinated Ce cation next-neighbor of the highest raised surface oxygen was consistent with the reported partial occupation of the most stable 7-coordinated Ce(4f) state of the reduced $Ce_{0.75}Zr_{0.25}O_2(111)$ and $CeO_2(111)$ surfaces.[7,53]

3.6. Discussion. The analysis of the different studied Ni interactions on(in) the $Ce_{0.75}Zr_{0.25}O_2(111)$ slab indicated that Ni interactions with Ce cations were unfavorable, in good agreement with the reported repulsive character of Ni−Ce interactions.[35] On the contrary, Ni adsorption/absorption's stability was driven by the bonding of Ni to oxygen atoms located near Zr cations, with the developing of strong Ni−support interactions. Besides, from the adsorption/absorption's energy calculations emerged the following preference order for the more stable Ni interactions: adsorption of a single Ni atom on the bare slab ($\Delta E_{ads,Ni} = -4.21$ eV) > adsorption of Ni_4 clusters on the bare slab ($\Delta E_{ads,Ni} = -3.89$ eV/Ni atom) > absorption of a single Ni atom into the bare slab ($\Delta E_{abs,Ni} = -3.88$ eV).

The most favorable of these interactions was the deposition of a single Ni atom on the surface O−O bridge site which nearest-neighbor metal atom is a Zr cation ($\Delta E_{ads,Ni} = -4.21$ eV). This suggested that the lower the content of nickel in the catalysts was, the stronger the interaction between Ni and the support became, as concluded from characterization results of Ni/CeO_2-ZrO_2 materials.[55]

Our DFT+U Ni adsorption/absorption results also showed that the deposition of Ni_4 clusters and the insertion of a Ni atom into the $Ce_{0.75}Zr_{0.25}O_2(111)$ slab were very likely occurrences. We calculated similar energy values (~-3.9 eV) for these Ni

Figure 8. Front view of the relaxation caused by Ni clusters adsorption on the $Ce_{0.75}Zr_{0.25}O_2(111)$ surface.

Figure 9. Side view of the relaxation caused by Ni clusters adsorption on the $Ce_{0.75}Zr_{0.25}O_2(111)$ surface. The dotted line indicates the position of the top metal cations. The region shown in the side view is also indicated between red lines in the front view on the right.
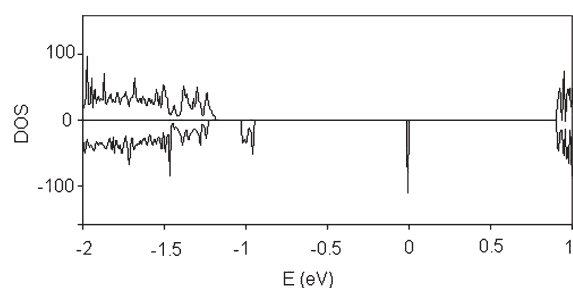
Figure 10. Spin-polarized density of states plot obtained for a single Ni atom adsorbed on the O—O bridge site W on the $Ce_{0.75}Zr_{0.25}O_2(111)$ surface.

interactions, which resulted only 0.32 eV (~7%) less stable than the most favorable single Ni atom deposition on the surface. The formation of Ni_4 species on the Ce—Zr oxide, 1.46 eV more favorable than in vacuum, was mainly facilitated by the Zr dopant; which acted as nucleation center for Ni clustering. Experimentally, the deposition of small Ni particles on CeO_2—ZrO_2 solid solutions has been related to the content of Zr dopant.[19,20,22,23] It was reported that CeO_2—ZrO_2 mixed oxide supports dispersed well the Ni particles,[20,22] forming crystallites of small average diameter,[19] and that finely dispersed Ni particles (active sites) increased with the raising of Zr content.[19,23] We have also realized that the meaningful possibility of Ni insertion into the subsurface layers of the $Ce_{0.75}Zr_{0.25}O_2$ solid solution was facilitated by the presence of Zr dopant. Ni located between two oxygen layers at 2.8 Å of a zirconium, the Ni nearest-neighbor metal cation, developed strong interactions with the surrounding O and Zr ions. The incorporation of some Ni into the CeO_2—ZrO_2 supports has been related to the formation of relatively small and finely dispersed Ni particles.[55] Particularly, the possibility of Ni entering into the lattice of the $Ni/Ce_{0.75}Zr_{0.25}O_2$ solid solution was also associated to the enhanced dispersion of Ni on the surface.[56] Therefore, our findings could be taken as indications of dispersed Ni species formation on the $Ce_{0.75}Zr_{0.25}O_2(111)$ surface, in agreement with experimental reports which have been connected the deposition of finely dispersed Ni particles to the content of Zr dopant and the occurrence of Ni entering into the lattice of CeO_2—ZrO_2 mixed oxides.[19,20,22,23,55,56]

The theoretical ab initio calculations could contribute to the understanding of Ni/CeO_2—ZrO_2 catalysts behavior through the description, at fundamental level, not only of Ni interactions with the support but also of the resulting atomic and electronic structures modifications. Looking at the atomic modifications, we underlined that Ni atoms bonded preferentially to oxygen anions located near the Zr dopant, and consequently the Ce—Zr mixed oxide structure experienced important relaxations. Due to Ni adsorption, the oxygens connected to Ni were pulled 0.6 Å of the surface. The interaction of a second Ni on the O—O bridge sites moved their bonded oxygens 1.35 Å out of the surface. After Ni insertion into the slab, the spacing between the second and third oxygen layers increased about 90% and the surface oxygen neighboring Ni ascended up to 1.14 Å. Electronically, the removal of oxygen atoms from the CeO_2 surface, forming anion vacant sites, has been related to the ability of cerium to easily adjust its electron configuration to best fit the immediate environment.[29,31,44,45,53] In Zr-doped CeO_2 solids, the formation of anion vacancies and the mobility of lattice oxygens were significantly enhanced by the distortion of the CeO_2 lattice.[7,30]

In all these materials, the creation of surface oxygen vacancies caused the simultaneous condensation of electrons into localized Ce(f)-level traps. Our density of states (DOS) plot of the $Ni_W/Ce_{0.75}Zr_{0.25}O_2$ system showed the rise of two peaks between the valence band and the empty conduction band: a broad peak at lower energy corresponding to the Ni(3d)—O(2p) overlapping, and a sharp peak at higher energy made of Ce(4f) orbitals. In our DOS plot, the higher energy peak mainly came from the electron transference of the most relaxed surface oxygen to a neighboring Ce cation. The analyses of the atomic modifications, caused by Ni adsorption/absorption interactions on(in) $Ce_{0.75}Zr_{0.25}O_2$ mixed oxides, have also shown important movement of inner layer oxygens coming up to the surface anion holes originated by Ni interactions. These displacements could have contributed to the observed electron localization on Ce(4f) orbitals, as reported for the diffusive movement of an oxygen atom toward the surface of CeO_2.[57]

Our study of Ni interactions on(in) the $Ce_{0.75}Zr_{0.25}O_2(111)$ system revealed a strong correlation between the structural and electronic properties. Ni interactions caused lattice strain with important relaxations of surface and subsurface ions, which resulted in the moving of bulk oxygens toward the surface, the pulling of the surface of the oxygen anions located near the Zr dopant, the enlargement of Ce—O and Zr—O bonds length with their consequent weakening, and also the modification of the $Ce_{0.75}Zr_{0.25}O_2$ insulator character through the electron population of Ce(4f) orbitals. Ni/CeO_2—ZrO_2 solid solutions have gained great attention during the past years, mainly due to the high activity and resistance to coke formation of these materials. The redox reactions and structural properties of Ni/CeO_2—ZrO_2 catalysts were mainly related to their behavior in methane reforming reactions.[13,15,58] The notable performance of these catalysts was connected with the couples Ce^{4+}/Ce^{3+}, and the reducibility and consequent oxygen mobility. Strong Ni—support interactions and Ni incorporation into the CeO_2—ZrO_2 mixed oxides lattices, which enhanced the reducibility and helped to produce mobile oxygens during methane reactions, were also related to the enhanced catalytic activity of Ni/CeO_2—ZrO_2 materials.[21,22,59] Our investigation of the $Ni/Ce_{0.75}Zr_{0.25}O_2$ system revealed important modifications caused by Ni adsorption/absorption interactions on the atomic and electronic structures. In spite of the lack of a detailed study about oxygen vacancies formation in this system, we found some interesting indications of surface and bulk oxygens' relaxations' influence in $Ce_{0.75}Zr_{0.25}O_2$ reducibility and Ce^{4+}/Ce^{3+} reactions. In that sense, our theoretical results could also be related to the catalytic activity of the Ni/CeO_2—ZrO_2 materials.

4. CONCLUSIONS

In this work, we have performed DFT+U quantum periodic calculations to analyze the energetics of Ni interactions on the $Ce_{0.75}Zr_{0.25}O_2(111)$ surface and the modifications in the atomic and electronic structures of the Ce—Zr mixed oxide support.

The comparison of the calculated Ni adsorption/absorption's energy values showed that the most stable interaction corresponded to a single Ni adsorbed on O—O bridge sites. In the $Ce_{0.75}Zr_{0.25}O_2(111)$ slab, Ni could also stabilize as Ni_4 species deposited on the surface or as Ni cation inserted into the subsurface layers.

The results showed that Ni atoms bonded preferentially to oxygen anions located near the Zr dopant and caused an important relaxation of the Ce—Zr mixed oxide structure, involving

7463

dx.doi.org/10.1021/jp1108703 |J. Phys. Chem. C 2011, 115, 7456–7465

not only surface Ce, Zr, and O ions but also O anions of the inner layers. The density of states of Ni adsorbed on O—O bridge sites showed the partial occupation of the 4f states of a cerium cation, situated near the most distorted surface oxygen anion, and could be interpreted as some extend reduction of the $Ce_{0.75}Zr_{0.25}O_2(111)$ slab.

Our theoretical calculations indicated that nickel interactions were influenced by Zr dopant, with the Zr doping centers facilitating Ni deposition as small clusters and also Ni insertion between two oxygen inner layers. These findings could be related to the reported tendency of Ni to adsorb as finely dispersed Ni particles on CeO_2—ZrO_2 mixed oxides, which was associated to the supports content of Zr dopant and the occurrence of Ni entering into their lattices. Besides, Ni adsorption/absorption interactions caused important relaxations of surface and inner layers anions and reduction to some extent of the $Ce_{0.75}Zr_{0.25}O_2$ structure, which could also modify the release of surface oxygens, and thus be related to the catalytic behavior of Ni/CeO_2—ZrO_2 solid solutions.

■ AUTHOR INFORMATION

Corresponding Author
*E-mail: beatriz@di.fcen.uba.ar.

■ ACKNOWLEDGMENT

■ REFERENCES

(1) Trovarelli, A. *Catalysis by Ceria and Related Materials, Catalytic Science Series*; Imperial College Press: London, 2002.

(2) Aneggi, E.; Boaro, M.; Leitenburg, C.; Dolcetti, G.; Trovarelli, A. *J. Alloys Comput.* **2006**, *408*, 1096.

(3) Kašpar, J.; Fornasiero, P.; Graziani, M. *Catal. Today* **1999**, *50*, 285.

(4) Rostrup-Nielsen, J.; Sehested, J.; Nørskov, J. K. *Adv. Catal.* **2002**, *47*, 65.

(5) Rostrup-Nielsen, J. *Catal. Today* **2009**, *145*, 72.

(6) Tang, S.; Lin, J.; Tan, K. L. *Catal. Lett.* **1998**, *51*, 169.

(7) Yang, Z.; Wei, Y.; Fu, Z.; Hermansson, K. *Surf. Sci.* **2008**, *602*, 1199.

(8) Fornasiero, P.; Di Monte, R.; Rao, G.; Kašpar, J.; Meriani, S.; Trovarelli, A.; Graziani, M. *J. Catal.* **1995**, *151*, 168.

(9) Fornasiero, P.; Balducci, G.; Di Monte, R.; Kašpar, J.; Sergo, V.; Gubitosa, G.; Ferrero, A.; Graziani, M. *J. Catal.* **1996**, *164*, 173.

(10) González-Velasco, J.; Gutiérrez-Ortiz, M.; Marc, J.; Botas, J.; González-Marcos, M.; Blanchard, G. *Appl. Catal. B: Environ.* **1999**, *22*, 167.

(11) Hori, C.; Permana, H.; Ng, K.; Brenner, A.; More, K.; Rahmoeller, K.; Belton, D. *Appl. Catal. B: Environ.* **1998**, *16*, 105.

(12) Kašpar, J.; Di Monte, R.; Fornasiero, P.; Graziani, M.; Bradshaw, H.; Norman, C. *Top. Catal.* **2001**, *16*, 83.

(13) Kim, T.; Vohs, J.; Gorte, R. *Ind. Eng. Chem. Res.* **2005**, *45*, 5561.

(14) Shah, P.; Kim, T.; Zhou, G.; Fornasiero, P.; Gorte, R. *Chem. Mater.* **2006**, *18*, 5363.

(15) Zhou, G.; Shah, P.; Kim, T.; Fornasiero, P.; Gorte, R. *Catal. Today* **2007**, *123*, 86.

(16) Shang, Q.; Shen, M.; Wen, J.; Wang, J.; Fe, Y. *J. Rare Earths* **2008**, *26*, 347.

(17) Dajiang, M.; Chen, Y.; Junbo, Z.; Zhenling, W.; Di, M.; Maochu, G. *J. Rare Earths* **2007**, *25*, 311.

(18) Wang, J.; Tai, Y.; Dow, W.; Huang, T. *Appl. Catal. A: Gen.* **2001**, *218*, 69.

(19) Xu, S.; Wang, X. *Fuel* **2005**, *84*, 563.

(20) Pengpanich, S.; Meeyoo, V.; Rirksomboon, T. *Catal. Today* **2004**, *93—95*, 95.

(21) Dong, W.; Jun, K.; Roh, H. *Catal. Lett.* **2002**, *78*, 215.

(22) Roh, H.; Koo, K.; Yoon, W. *Catal. Today* **2009**, *146*, 71.

(23) Kambolis, A.; Matralis, H.; Trovarelli, A.; Papadopoulou, Ch. *Appl. Catal. A: Gen.* **2010**, *377*, 16.

(24) Larrondo, S.; Vidal, M.; Irigoyen, B.; Craievich, A.; Lamas, D.; Fábregas, I.; Lascalea, G.; Walsöe de Reca, N.; Amadeo, N. *Catal. Today* **2005**, *107—108*, 53.

(25) Lamas, D.; Cabezas, M.; Fábregas, I.; Walsöe de Reca, N.; Kodjaian, A.; Vidal, A.; Amadeo, N.; Larrondo, S. *ECS Trans.* **2007**, *7*, 961.

(26) Horváth, A.; Stefler, G.; Geszti, O.; Kienneman, A.; Pietraszek, A.; Guczi, L. *Catal. Today* **2010**, available online Sept 28.

(27) Nichio, N.; Casella, M.; Ferretti, O.; González, M.; Nicot, C.; Moraweck, B.; Frety, R. *Catal. Lett.* **1996**, *42*, 65.

(28) Hu, Y.; Ruchenstein, E. *Catal. Lett.* **1996**, *36*, 145.

(29) Huang, M.; Fabris, S. *J. Phys. Chem. C* **2008**, *112*, 8643.

(30) Yang, Z.; Lu, Z.; Luo, G.; Hermansson, K. *Phys. Rev. B* **2007**, *76*, 75421.

(31) Castleton, C.; Kullgren, J.; Hermansson, K. *J. Chem. Phys.* **2007**, *127*, 244704.

(32) Jung, C.; Tsuboi, H.; Koyama, M.; Kubo, M.; Broclawik, E.; Miyamoto, A. *Catal. Today* **2006**, *111*, 322.

(33) Alfredsson, M.; Catlow, C. *Phys. Chem. Chem. Phys.* **2002**, *4*, 6100.

(34) Lu, Z.; Yang, Z. *Eur. Phys. J. B* **2008**, *63*, 455.

(35) Chafi, Z.; Keghouche, N.; Minot, C. *Surf. Sci.* **2007**, *601*, 2323.

(36) Wang, X.; Shen, M.; Wang, J.; Fabris, S. *J. Phys. Chem. C* **2010**, *114*, 10221.

(37) Kresse, G.; Furthmuller, J. *Comput. Mater. Sci.* **1996**, *6*, 15.

(38) Kresse, G.; Hafner, J. *Phys. Rev. B: Condens. Matter. Mater. Phys.* **1993**, *47*, 558.

(39) Perdew, J.; Burke, K.; Ernzerhof, M. *Phys. Rev. Lett.* **1996**, *77*, 3865.

(40) Kresse, G.; Joubert, D. *Phys. Rev. B: Condens. Matter Mater. Phys.* **1999**, *59*, 1758.

(41) Monkhorst, H.; Pack, J. *Phys. Rev. B: Condens. Matter Mater. Phys.* **1976**, *13*, 5188.

(42) Dudarev, S.; Botton, G.; Savrasov, S.; Humphreys, C.; Sutton, A. *Phys. Rev. B: Condens. Matter Mater. Phys.* **1998**, *57*, 1505.

(43) Anisimov, V.; Zaanen, J.; Andersen, O. *Phys. Rev. B: Condens. Matter Mater.* **1991**, *44*, 943.

(44) Nolan, M.; Parker, S.; Watson, G. *Surf. Sci.* **2005**, *595*, 223.

(45) Nolan, M.; Grigoleit, S.; Sayle, D.; Parker, S.; Watson, G. *Surf. Sci.* **2005**, *576*, 217.

(46) Eyring, L. *Handbook on the Physics and Chemistry of Rare Earths*; Gschneider, K. A.; Eyring, L., Eds.; North-Holland: Amsterdam, 1979.

(47) Rodriguez, J.; Hanson, J.; Kim, J.; Liu, G.; Iglesias-Juez, A.; Fernández-García, M. *J. Phys. Chem. B* **2003**, *107*, 3535.

(48) Vlaic, G.; Di Monte, R.; Fornasiero, P.; Fonda, E.; Kašpar, J.; Graziani, M. *J. Catal.* **1999**, *182*, 378.

(49) Markovits, A.; Skalli, M.; Minot, C.; Pacchioni, G.; López, N.; Illas, F. *J. Chem. Phys.* **2001**, *115*, 8172.

(50) Yang, Z.; Woo, T.; Hermansson, K. *J. Chem. Phys.* **2006**, *124*, 224704.

(51) Chettibi, S.; Wojcieszak, R.; Boudjennad, E.; Belloni, J.; Bettehar, M.; Keghouche, N. *Catal. Today* **2006**, *113*, 157.

(52) Wuilloud, E.; Delley, B.; Schneider, W. D.; Baer, Y. *Phys. Rev. Lett.* **1984**, *53*, 202.

(53) Conesa, J. C. *Catal. Today* **2009**, *143*, 315.

(54) Zhou, Y.; Perket, J.; Crooks, A.; Zhou, J. *J. Phys. Chem. Lett.* **2010**, *1*, 1447.

(55) Dong, W.; Roh, H.; Jun, K.; Park, S.; Oh, Y. *Appl. Catal. A: Gen.* **2002**, *226*, 63.

(56) Chen, J.; Wu, Q.; Zhang, J.; Zhang, J. *Fuel* **2008**, *87*, 2901.

(57) Skorodumova, N.; Simak, S.; Lundqvist, B.; Abrikosov, I.; Johansson, B. *Phys. Rev. Lett.* **2002**, *89*, 166601.

(58) Ocampo, F.; Louis, B.; Kiwi-Minsker, L.; Roger, A. *Appl. Catal. A: Gen.* **2011**, *392*, 36.

(59) Roh, H.; Potdar, H.; Jun, K. *Catal. Today* **2004**, *93*, 39.